Temperature-Dependent Spin Transport and Current-Induced Torques in Superconductor-Ferromagnet Heterostructures

M. Müller,[1,2,*] L. Liensberger,[1,2] L. Flacke,[1,2] H. Huebl,[1,2,3] A. Kamra,[4] W. Belzig,[5] R. Gross,[1,2,3] M. Weiler,[1,2,‡] and M. Althammer[1,2,†]

[1]*Walther-Meißner-Institut, Bayerische Akademie der Wissenschaften, 85748 Garching, Germany*
[2]*Physik-Department, Technische Universität München, 85748 Garching, Germany*
[3]*Munich Center for Quantum Science and Technology (MCQST), Schellingstraße 4, 80799 München, Germany*
[4]*Center for Quantum Spintronics, Department of Physics, Norwegian University of Science and Technology, NO-7491 Trondheim, Norway*
[5]*Fachbereich Physik, Universität Konstanz, 78457 Konstanz, Germany*

(Received 30 July 2020; revised 1 December 2020; accepted 21 January 2021; published 22 February 2021)

We investigate the injection of quasiparticle spin currents into a superconductor via spin pumping from an adjacent ferromagnetic metal layer. To this end, we use NbN-$Ni_{80}Fe_{20}$(Py) heterostructures with a Pt spin sink layer and excite ferromagnetic resonance in the Permalloy layer by placing the samples onto a coplanar waveguide. A phase sensitive detection of the microwave transmission signal is used to quantitatively extract the inductive coupling strength between the sample and the coplanar waveguide, interpreted in terms of inverse current-induced torques, in our heterostructures as a function of temperature. Below the superconducting transition temperature T_c, we observe a suppression of the dampinglike torque generated in the Pt layer by the inverse spin Hall effect, which can be understood by the changes in spin current transport in the superconducting NbN layer. Moreover, below T_c we find a large fieldlike current-induced torque.

DOI: 10.1103/PhysRevLett.126.087201

Over the last decade, the field of superconducting spintronics [1–11] has attracted increasing attention due to the novel and beneficial spin transport properties related to quasiparticles [12–15] and spin-triplet Cooper pairs in superconductors (SCs) [6,16–20]. Among those, charge-to-spin current interconversion and the associated spin-orbit torque effects allow for the control of magnetization and its dynamics. Investigations in this direction began with dc-transport experiments in SC lateral spin valve structures and reported changes in spin signal and spin diffusion length λ_S [21–23] below the SC transition temperature T_c.

Recent experiments [17,24–30] focused on the nonequilibrium magnetization dynamics of a ferromagnetic metal (FM) layer adjacent to a SC film. Here, changes of the parameters describing magnetization dynamics below T_c provide insight into the spin injection in SCs via spin pumping [17,25–28,30]. Experiments analyzing the magnetization damping using ferromagnetic resonance (FMR) techniques in SC-FM hybrid systems close to T_c allowed to explore several phenomena, ranging from a monotonic reduction of spin pumping due to a freeze-out of quasiparticles (QPs) [25] over the manifestation of a coherence peak slightly below T_c [26], to the spin pumping mediated by spin-triplet Cooper pairs [17].

To clarify the origin of these competing results, we here present a systematic study of the magnetization dynamics of FM-SC heterostructures as a function of temperature at and below T_c. This includes the investigation of linear spin-orbit torques present in these multilayers by employing broadband ferromagnetic resonance (bbFMR) experiments in combination with the phase sensitive detection of the microwave transmission signal. This approach allows us to simultaneously detect the electrical ac currents due to magnetization dynamics. These ac currents can arise due to inverse spin-orbit torques (iSOT), as well as classical electrodynamics (i.e., Faraday's law). For concise notation, we will quantify them in terms of σ^{SOT} in accordance with previous work [31]. We are hence able to quantify the impact of an adjacent SC film on both the magnetization dynamics (e.g., FMR linewidth) and the fieldlike and dampinglike σ^{SOT} in SC-FM heterostructures. For the latter, we expand the inductive coupling analysis reported in Ref. [31] to account for SC layers. In this way, we establish a new powerful method to study nonequilibrium spin transport in SCs.

For this Letter, we fabricate heterostructures based on NbN, Py, Pt, and TaO_x, which are *in situ* deposited on a thermally oxidized Si (100) substrate by dc magnetron sputtering. [For more details on the deposition process, see the Supplemental Material (SM) [32]]. While the thickness of NbN (16 nm) and Py (6 nm) are constant, the Pt, acting as spin sink, is varied in thickness and position within the layer sequence [see Fig. 1(a)]. The layer thickness of NbN was chosen to be as thin as possible while maintaining a reasonable T_c, whereas the layer thickness of Py was selected to ensure a good signal-to-noise ratio. TaO_x is used

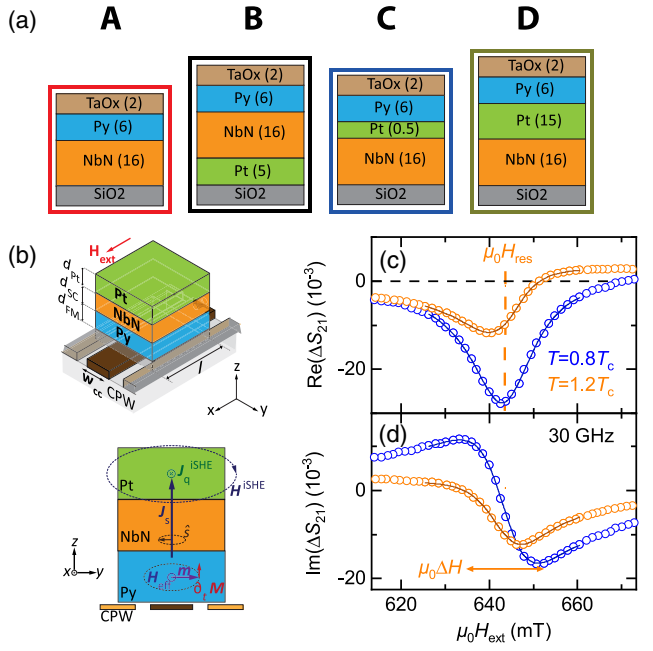

FIG. 1. (a) Layer stack of samples investigated in this Letter. Numbers show the layer thicknesses in nm. For bbFMR, the samples are mounted facedown on top of a coplanar waveguide. (b) Sketch of the measurement geometry for in-plane bbFMR and schematic illustration for the generation of the charge current density $\boldsymbol{J}_q^{\mathrm{iSHE}}$ by ac iSHE. The ac flux $\boldsymbol{H}^{\mathrm{iSHE}}$ generated by $\boldsymbol{J}_q^{\mathrm{iSHE}}$ is coupled into the CPW. In (c) and (d), the change in complex transmission is plotted versus the applied external field $\mu_0 H_{\mathrm{ext}}$ both slightly above and below T_c for sample B ($T_c = 9.0$ K). Both the FMR amplitude and phase exhibit clear changes in the SC state. The lines in (c) and (d) represent Polder susceptibility χ fits to Eq. (S21).

as the cap layer to prevent the oxidation of the heterostructure. AFM surface roughness and x-ray-diffraction scans revealed a low surface roughness (below the detection limit, that is, < 300 pm) in our samples (see the SM, Figs. S2 and S3). We perform bbFMR measurements in a cryogenic environment over a broad temperature range. A sketch of the measurement geometry is shown in Fig. 1(b). The samples were mounted facedown onto a coplanar waveguide (CPW), of which we record the complex microwave transmission S_{21} using a vector-network analyzer (VNA). In particular, we set fixed microwave frequencies f (10 GHz $\leq f \leq$ 36 GHz) and measure as a function of the applied external magnetic field H_{ext} applied along the $\hat{\boldsymbol{e}}_x$ direction at a VNA output power of 1 mW. At such low power, all dynamics are in the linear response regime. We first focus on sample B. For $T > T_c$, the magnetization dynamics excited in the FM using FMR pump a spin current density $\boldsymbol{J}_s$ across the FM-SC interface ($T > T_c$) and the SC into the adjacent Pt layer as illustrated in the inset of Fig. 1(b). In the Pt layer, $\boldsymbol{J}_s$ is absorbed and converted into a charge current $\boldsymbol{J}_q$ via the inverse spin Hall effect (iSHE), where we assume a vanishing iSHE contribution from the SC layer. This spin pumping effect manifests itself on the one hand as an additional contribution to the damping of the FMR as it represents an additional relaxation channel for angular momentum [24]. On the other hand, the ac magnetic field H^{iSHE} generated via the iSHE induced charge current $\boldsymbol{J}_q^{\mathrm{iSHE}}$ is inductively coupled into the CPW and thus can be detected by the VNA [31]. Note that all experiments are performed for an in-plane geometry ($\boldsymbol{H}_{\mathrm{ext}} \| \hat{\boldsymbol{e}}_x$) to avoid the formation of vortices in the SC state. Figure 1(c), (d) show data for the background-corrected change in transmission $\Delta S_{21} = \Delta S_{21}/\Delta S_{21}^0 - 1$ [see Eq. (S21)] in proximity to FMR for temperatures slightly above (orange) and below T_c (blue). The raw data in Fig. 1(c), (d) reveal that the SC transition significantly modifies the detected ΔS_{21} spectra. In the normal state ($T > T_c$), the asymmetric line shape of $\mathrm{Re}(\Delta S_{21})$ matches that of a (Py-Pt) sample in Ref. [31], where the inductive coupling between currents generated in a normal metal (NM) by iSOT and a CPW were investigated at room temperature.

Below T_c, the diplike shape of $\mathrm{Re}(\Delta S_{21})$ [blue circles in Fig. 1(c)], indicative of the absence of spin-to-charge current conversion, is mostly restored. We also observe an enhanced FMR amplitude, suggesting a modified inductive coupling $\tilde{L}$ between the sample and CPW in the SC state. To extract the resonance field H_{res} and linewidth ΔH, we fit our raw data to the Polder susceptibility χ in Eq. (S21) and then employ a data analysis procedure based on [31] to extract the normalized inductance $\tilde{L} = L/\chi$ with Eq. (S27) (see the SM). By normalizing with χ, the resulting $\tilde{L}$ is independent of magnetization dynamics parameters like linewidth ΔH and merely sensitive to charge currents induced by magnetization dynamics in our samples [59]. Following Berger *et al.* [31], $\tilde{L}(f)$ is modeled as

$$\begin{aligned}\tilde{L}(f) &= \tilde{L}_0 + \tilde{L}_j(f) \\ &= \tilde{L}_0 + f \cdot [\mathrm{Re}(\Delta\tilde{L}_j)\epsilon_r(f) + i \cdot \mathrm{Im}(\Delta\tilde{L}_j)\epsilon_i(f)]. \quad (1)\end{aligned}$$

Above T_c, $\tilde{L}_0$ is a measure of the coupling strength between the FM and the CPW and must be strictly real for $f \to 0$ Hz, which is well met in our samples, while $\tilde{L}_j$ accounts for the flux generated by ac charge currents in the adjacent NM-SC layer. $\Delta\tilde{L}_j$ denotes the linear frequency dependence of $\tilde{L}_j$ [see the SM for a derivation of Eq. (1)]. We further account for elliptical magnetization precession with the in-plane correction factors $\epsilon_r(f)$ and $\epsilon_i(f)$ for the real and imaginary parts, respectively [for details, see Eq. (S40) in the SM]. We plot the extracted $\tilde{L}_0$ and $\tilde{L}_j$ as a function of reduced temperature for the Pt-NbN-Py trilayer in Fig. 2(a), (b), respectively. Exemplary raw fitting data for $\tilde{L}(f)$ for all samples investigated are presented in the SM.

Compared to $\tilde{L}_0$ at $T > T_c$, we observe in Fig. 2(a) a strongly enhanced coupling strength manifesting itself in a large $\mathrm{Re}(\tilde{L}_0)$ between the sample and CPW in the SC state

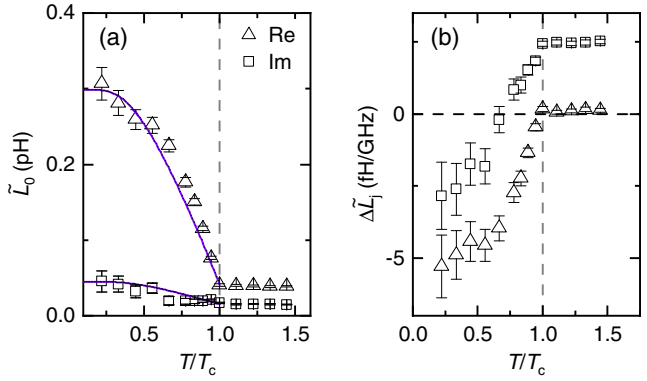

FIG. 2. Inductive coupling parameters for sample B with the stack sequence Pt (5 nm)–NbN (16 nm)–Py (6 nm)–TaO_x (2 nm) plotted as a function of reduced temperature around T_c. In (a), we plot the real (triangles) and imaginary (squares) parts of the inductive coupling offset $\tilde{L}_0$. The lines indicate the scaled superfluid condensate density n_s following BCS theory. In (b), we show the real (triangles) and imaginary (squares) parts of the complex linear frequency dependence $\Delta\tilde{L}_j$ of the normalized inductance $\tilde{L}$. The error bars originate from fitting the extracted raw data for $\tilde{L}$ with Eq. (1).

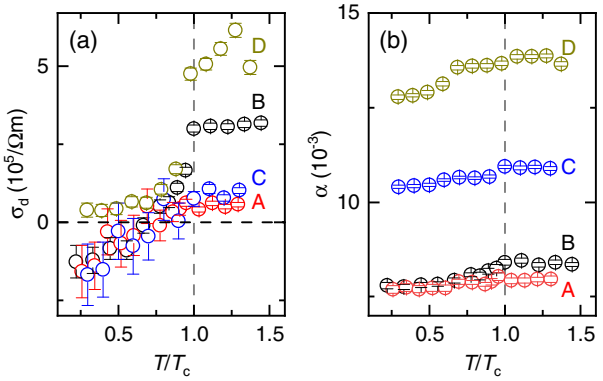

FIG. 3. (a) Dampinglike current-induced torque conductivity σ_d plotted as a function of T/T_c. In the normal state, the samples containing Pt exhibit large positive σ_d due to the iSHE in Pt. Below T_c, all samples exhibit a very similar decay of σ_d with decreasing T irrespective of Pt spin sink layer. (b) Temperature dependence of the Gilbert damping α in the SC state as a function of T/T_c. The apparent decrease of α is due to the suppression of spin pumping into the SC due to the freeze-out of thermally excited quasiparticles. The error bars originate from fitting the extracted raw data for $\tilde{L}$ with Eq. (S42) (a) and Eq. (S17) for $\Delta H(f)$ (b).

that gradually increases with decreasing T. Simultaneously, $\mathrm{Im}(\tilde{L}_0) > 0$ is observed for $T \mapsto 0$, while $\mathrm{Im}(\tilde{L}_0) \approx 0$ for $T > T_c$. Both observed effects are manifestations of superconductivity in NbN. In the SC state, image currents in the NbN layer mirror the external driving field of the CPW [60] and keep the SC in the Meißner phase. Consequently, the sandwiched FM layer is driven from both sides with an enlarged net oscillatory driving field $\boldsymbol{h}_{\mathrm{rf}}$, leading to the enhanced inductive coupling between the sample and CPW. The nonzero $\mathrm{Im}(\tilde{L}_0)$ below T_c is attributed to the complex surface impedance $Z_{\mathrm{eff}}(\omega)$ in the SCs (see the SM).

We now turn to the linear contribution to $\tilde{L}_j$, $\Delta\tilde{L}_j$, shown in Fig. 2(b). Note that $\tilde{L}_j \neq 0$ is obtained whenever electrical ac currents are generated in the samples by magnetization dynamics $\boldsymbol{m}(t)$. We find that both $\mathrm{Re}(\Delta\tilde{L}_j)$ (triangles, caused by currents in quadrature with m_y) and $\mathrm{Im}(\Delta\tilde{L}_j)$ (squares, caused by currents in phase with m_y) change drastically just below T_c. The real and imaginary parts of $\tilde{L}_j$ are attributed to the manifestation of fieldlike and dampinglike inverse current-induced torques (for a detailed discussion, see the SM). For a quantitative analysis of these effects, we extract the SOT conductivities σ^{SOT} from $\tilde{L}_j$ by using the relation

$$\tilde{L}_j(f) = C \cdot f \cdot [-\epsilon_r(f)\sigma_f + i\epsilon_i(f)\sigma_d]. \tag{2}$$

Analogous to Ohm's law, they relate current to change in magnetization $\boldsymbol{J} \propto \sigma^{\mathrm{SOT}}\partial\boldsymbol{M}/\partial t$ [59]. The indices f and d denote the fieldlike and dampinglike spin-orbit torques, respectively. The fieldlike part σ_f denotes the inverse Rashba-Edelstein effect (iREE) [61,62] but also contains a Faraday contribution (magnetization dynamics in the FM induce dynamic charge currents in the adjacent NM). It is defined as $\sigma_f = (\sigma_f^{\mathrm{iREE}} - \sigma_f^{\mathrm{Faraday}})$, whereas σ_d is attributed to the iSHE. In our samples, the latter is dominated by the conversion of spin currents into charge currents in Pt. The proportionality constant C in Eq. (2) is defined in the SM [Eq. (S37)]. Furthermore, below T_c, we multiply an additional correction term to Eq. (2) to account for the altered net driving field strength $\boldsymbol{h}_{\mathrm{rf}}$ [Eq. (S42)].

The inductive coupling strength $\tilde{L}_j$ between NM and CPW is a linear function of σ^{SOT} [31]. The dampinglike and fieldlike current-induced torques σ_d and σ_f derived for the different samples are shown in Figs. 3 and 4, respectively. As shown in Fig. 3(a), for $T > T_c$, we observe large σ_d values for the samples B and D as expected due to the iSHE in Pt. In contrast, sample A (NbN-Py bilayer) exhibits only small positive σ_d values, which we attribute to spin pumping into the unoxidized fraction of the TaO_x cap layer. For sample C, we determine a low σ_d, indicating a reduction in the spin-to-charge current conversion due to the much lower thickness of the Pt layer. These results are in agreement with the expectations that Pt acts as a spin sink and efficiently converts spin into charge currents. Below T_c, σ_d rapidly decreases and eventually reaches a similar slightly negative value for samples A, B, and C, while staying slightly positive for sample D. There are two effects that affect σ_d in the SC state: First, there is a strongly modified spin transport carried by thermally excited QPs and, second, there is a shunting effect by the SC condensate. For sample B, the spin current has to pass the SC layer to reach the Pt layer such that altered spin transport properties in the SC play an important role in this case.

The observed changes for the SC-thick Pt-FM sample D, where the primary source of iSHE is the Pt layer and no spin current can reach the SC due to the low spin diffusion length λ_S in Pt, can be well explained by the SC acting as an electrical shunt, which reduces the charge current density $\boldsymbol{J}_q^{\mathrm{iSHE}}$ in Pt and as a result also σ_d. A strong reduction in the detected magnitude of the iSHE in Pt due to shunting effects when brought into contact with highly conductive Cu has been reported in Refs. [63,64]. Here, we observe an analog shunting effect for superconductors, giving rise to the same strong suppression of the iSHE. The small negative values of σ_d in samples A, B, and C below T_c are consistent with the quasiparticle mediated inverse spin Hall effect (QMiSHE) in the SC [65–68]. The negative spin Hall angle [69,70] and the associated QMiSHE in NbN have been observed via nonlocal dc transport measurements [70]. Remarkably, a diverging spin Hall angle resulting from intrinsic and side-jump contributions to the SHE compensates for a diminishing quasiparticle population with decreasing temperature (see the SM). A finite QMiSHE current is therefore expected in the SC state, as observed in Fig. 3(a). In sample D, the QMiSHE is absent as the spin current is entirely absorbed in the thick Pt layer. To support the validity of our approach and interpretation, we compare the dampinglike σ_d to the extracted Gilbert damping α of Py, which is plotted as a function of T/T_c in Fig. 3(b). Due to spin pumping, α also directly probes spin current transport in the heterostructure. The α value of sample A matches literature values well for the damping of Py thin films [71–75] and hence serves as our reference sample in the absence of spin pumping. Consequently, larger α in the other samples originates from spin pumping into Pt. Thus, we observe substantial spin pumping contributions at all temperatures for samples C and D. In the SC regime, the α values of sample B approach the values of our reference (sample A). This suggests a complete suppression of spin pumping into Pt at $T \ll T_c$. These results are in agreement with Ref. [25]. Furthermore, similar to Ref. [17], we detect an enhancement in the linewidth $\mu_0 \Delta H$ in the SC state at low frequencies in our samples. However, we can attribute this to an enlarged $\mu_0 H_{\mathrm{inh}}$. Consequently, our interpretation of the experimental observation differs from that given in Ref. [17], where an enhanced $\mu_0 \Delta H$ is attributed to spin-polarized supercurrents in SCs. However, we interpret the observed reduction of α in the SC state by a freeze-out of QP spin pumping (for a detailed comparison to Ref. [17], see the SM, Section 14). In sample C, the slight reduction of α below T_c is attributed to the blocking of spin currents at the NbN-Pt interface, whereas in sample D it is caused by the SC shunting effect leading to a reduction in the iSHE in Pt. The α values of samples C and D remain substantially larger than those of sample A even for $T < T_c$ because spin pumping into Pt is not affected by the superconducting NbN on the far interface. The direct detection of dissipative

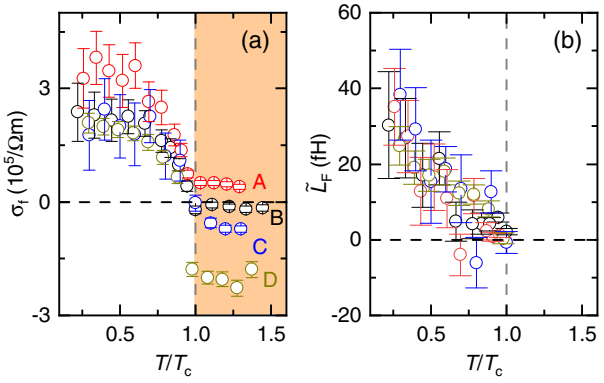

FIG. 4. (a) Extracted fieldlike current-induced torque σ_f plotted as a function of T/T_c. Due to a complex surface impedance $Z_{\mathrm{eff}}(\omega)$ in the SC, the Faraday contribution $\sigma_f^{\mathrm{Faraday}}$ creates an offset in $\mathrm{Im}(\tilde{L})$ and only affects σ_f above T_c. We marked the corresponding temperature range with an orange background. In the SC state, we detect a substantial positive σ_f. (b) Change in $\mathrm{Im}(\tilde{L})$ in the SC state due to SC Faraday currents. The error bars in (a) and (b) originate from fitting the extracted raw data for $(\tilde{L})$ with Eq. (S42).

spin currents via SOT in Fig. 3(a) is thus consistent with their indirect detection via FMR damping α in Fig. 3(b).

Apart from σ_d, originating from the iSHE, we can simultaneously extract σ_f generated by Faraday currents and fieldlike iSOT effects in the normal state. We plot the extracted σ_f for our samples in Fig. 4(a). Above T_c, we detect negative values for samples B, C, and D, attributed to Faraday currents in Pt, and a small positive σ_f for sample A, which indicates fieldlike iSOTs at the NbN-Py interface in the normal state. Below T_c, all samples exhibit a substantial positive σ_f that gradually increases for decreasing T. Here, the observed behavior of all samples is nearly independent of the inclusion and position of the Pt layer. For $T < T_c$, Faraday currents in the SC do not contribute to the slope of $\mathrm{Re}(\tilde{L})$ (and thus σ_f) but generate an offset $\tilde{L}_F$ in $\mathrm{Im}(\tilde{L})$ as illustrated in Fig. 4(b). This explains the vanishing disparity in $\sigma_f(T)$ for all samples below T_c with the simultaneous manifestation of $\tilde{L}_F$. Faraday currents are hence still present below T_c but now manifest themselves in $\tilde{L}_F$, because the SC now acts as an inductor and not a resistor [see the SM, Eq. (S44)]. The change in $\mathrm{Im}(\tilde{L}_0)$ due to Faraday currents in the SC is similar in all samples. Moreover, the positive σ_f for $T < T_c$ in Fig. 4(a) has the opposite sign compared to that expected from Faraday currents. The non-zero σ_f for $T \mapsto 0$ also cannot be attributed to the inverse Rashba-Edelstein effect [61,62] or the electromagnetic proximity effect [76,77] at the SC-FM interface, as the observed phenomenon is seemingly independent of the material adjacent to the SC and does not require direct contact between SC and FM. Having ruled out the common sources of fieldlike current-induced torques, we can merely speculate about the origin of the positive σ_f in the SC state in our samples. Potential

candidates to generate σ_f in these samples include the coherent motion of vortices in an rf field [78,79] as well as the impact of Meißner screening currents on the magnetization dynamics due to triplet superconductivity [17] or nonequilibrium effects [80].

In summary, we adapt the method outlined in Ref. [31] to detect the manifestation of substantial fieldlike and the reduction of dampinglike current-induced torques in FM-SC hybrids below T_c. Our observations on the dampinglike current-induced torques are consistent with a shunting effect of the SC and quasiparticle-mediated iSHE in NbN. In particular, we establish a complementary detection technique for the QMiSHE that corroborates a recent report [70]. The Gilbert damping $\alpha(T)$ demonstrates that spin current transport through the SC in FM-SC-Pt heterostructures is blocked below T_c, while spin pumping in the FM-Pt-SC layers is only weakly affected by the SC transition. The sizable fieldlike current-induced torque below T_c does not originate from Faraday currents or interfacial iSOTs. This as yet unexplained observation raises interesting questions regarding the theoretical understanding of spin current transport in FM-SC hybrids. Our method enables the study of manifold theoretically proposed exotic phenomena at the SC-FM interface like, e.g., the generation of supercurrents by Rashba spin-orbit interaction [61,81], supercurrent-induced spin-orbit torques [82], or the theoretically proposed vortex spin Hall effect [83]. Using our method, these studies can be performed while simultaneously extracting key spectroscopic parameters such as Gilbert damping α and without requiring any sample patterning.

We acknowledge financial support by the Deutsche Forschungsgemeinschaft (DFG, German Research Foundation) via WE5386/4-1, WE5386/5-1, 425217212 SFB 1432, and Germanys Excellence Strategy EXC-2111-390814868 and the Research Council of Norway through its Centers of Excellence funding scheme, Project No. 262633, "QuSpin."

*Corresponding author.
manuel.mueller@wmi.badw.de
†Corresponding author.
matthias.althammer@wmi.badw.de
‡Present address: Fachbereich Physik and Landesforschungszentrum OPTIMAS, Technische Universität Kaiserslautern, Gottlieb-Daimler-Straße 46, 67663 Kaiserslautern, Germany.

[1] S. K. Sinha, G. W. Crabtree, D. G. Hinks, and H. Mook, Phys. Rev. Lett. **48**, 950 (1982).
[2] S. S. Saxena, P. Agarwal, K. Ahilan, F. M. Grosche, R. K. W. Haselwimmer, M. J. Steiner, E. Pugh, I. R. Walker, S. R. Julian, P. Monthoux, G. G. Lonzarich, A. Huxley, I. Sheikin, D. Braithwaite, and J. Flouquet, Nature (London) **406**, 587 (2000).
[3] F. Levy, Science **309**, 1343 (2005).
[4] J. S. Jiang, D. Davidović, D. H. Reich, and C. L. Chien, Phys. Rev. Lett. **74**, 314 (1995).
[5] M. G. Khusainov and Y. N. Proshin, Phys. Rev. B **56**, R14283 (1997).
[6] J. Linder and J. W. A. Robinson, Nat. Phys. **11**, 307 (2015).
[7] K. Ohnishi, S. Komori, G. Yang, K.-R. Jeon, L. A. B. O. de Olthof, X. Montiel, M. G. Blamire, and J. W. A. Robinson, Appl. Phys. Lett. **116**, 130501 (2020).
[8] N. O. Birge, Phil. Trans. R. Soc. A **376**, 20150150 (2018).
[9] M. Eschrig, Rep. Prog. Phys **78**, 104501 (2015).
[10] F. S. Bergeret, A. F. Volkov, and K. B. Efetov, Rev. Mod. Phys. **77**, 1321 (2005).
[11] A. I. Buzdin, Rev. Mod. Phys. **77**, 935 (2005).
[12] M. Inoue, M. Ichioka, and H. Adachi, Phys. Rev. B **96**, 024414 (2017).
[13] T. Kato, Y. Ohnuma, M. Matsuo, J. Rech, T. Jonckheere, and T. Martin, Phys. Rev. B **99**, 144411 (2019).
[14] M. Umeda, Y. Shiomi, T. Kikkawa, T. Niizeki, J. Lustikova, S. Takahashi, and E. Saitoh, Appl. Phys. Lett. **112**, 232601 (2018).
[15] J. P. Morten, A. Brataas, G. E. W. Bauer, W. Belzig, and Y. Tserkovnyak, Europhys. Lett. **84**, 57008 (2008).
[16] R. S. Keizer, S. T. B. Goennenwein, T. M. Klapwijk, G. Miao, G. Xiao, and A. Gupta, Nature (London) **439**, 825 (2006).
[17] K.-R. Jeon, C. Ciccarelli, A. J. Ferguson, H. Kurebayashi, L. F. Cohen, X. Montiel, M. Eschrig, J. W. A. Robinson, and M. G. Blamire, Nat. Mater. **17**, 499 (2018).
[18] N. Banerjee, J. A. Ouassou, Y. Zhu, N. A. Stelmashenko, J. Linder, and M. G. Blamire, Phys. Rev. B **97**, 184521 (2018).
[19] N. Satchell and N. O. Birge, Phys. Rev. B **97**, 214509 (2018).
[20] N. Satchell, R. Loloee, and N. O. Birge, Phys. Rev. B **99**, 174519 (2019).
[21] N. Poli, J. P. Morten, M. Urech, A. Brataas, D. B. Haviland, and V. Korenivski, Phys. Rev. Lett. **100**, 136601 (2008).
[22] H. Yang, S.-H. Yang, S. Takahashi, S. Maekawa, and S. S. P. Parkin, Nat. Mater. **9**, 586 (2010).
[23] J. Y. Gu, J. A. Caballero, R. D. Slater, R. Loloee, and W. P. Pratt, Phys. Rev. B **66**, 140507(R) (2002).
[24] Y. Tserkovnyak, A. Brataas, and G. E. W. Bauer, Phys. Rev. B **66**, 224403 (2002).
[25] C. Bell, S. Milikisyants, M. Huber, and J. Aarts, Phys. Rev. Lett. **100**, 047002 (2008).
[26] Y. Yao, Q. Song, Y. Takamura, J. P. Cascales, W. Yuan, Y. Ma, Y. Yun, X. C. Xie, J. S. Moodera, and W. Han, Phys. Rev. B **97**, 224414 (2018).
[27] K.-R. Jeon, C. Ciccarelli, H. Kurebayashi, J. Wunderlich, L. F. Cohen, S. Komori, J. W. A. Robinson, and M. G. Blamire, Phys. Rev. Applied **10**, 014029 (2018).
[28] K.-R. Jeon, C. Ciccarelli, H. Kurebayashi, L. F. Cohen, X. Montiel, M. Eschrig, S. Komori, J. W. A. Robinson, and M. G. Blamire, Phys. Rev. B **99**, 024507 (2019).
[29] K.-R. Jeon, C. Ciccarelli, H. Kurebayashi, L. F. Cohen, X. Montiel, M. Eschrig, T. Wagner, S. Komori, A. Srivastava, J. W. A. Robinson, and M. G. Blamire, Phys. Rev. Applied **11**, 014061 (2019).

[30] K.-R. Jeon, C. Ciccarelli, H. Kurebayashi, L. F. Cohen, S. Komori, J. W. A. Robinson, and M. G. Blamire, Phys. Rev. B **99**, 144503 (2019).

[31] A. J. Berger, E. R. J. Edwards, H. T. Nembach, A. D. Karenowska, M. Weiler, and T. J. Silva, Phys. Rev. B **97**, 094407 (2018).

[32] See Supplemental Material at http://link.aps.org/supplemental/10.1103/PhysRevLett.126.087201, which includes Refs. [33–58], for a detailed description of the sample fabrication procedure, data analysis procedure and fitting routine, and an illustration of the raw data for the inductive coupling. Furthermore, we show the magnetization dynamics and iSOT parameters of all samples in the full temperature range and also include some results using a different FM layer ($Co_{25}Fe_{75}$).

[33] G. Horn and E. Saur, Z. Phys. A **210**, 70 (1968).

[34] D. Hazra, N. Tsavdaris, S. Jebari, A. Grimm, F. Blanchet, F. Mercier, E. Blanquet, C. Chapelier, and M. Hofheinz, Supercond. Sci. Technol. **29**, 105011 (2016).

[35] M. Chand, A. Mishra, Y. M. Xiong, A. Kamlapure, S. P. Chockalingam, J. Jesudasan, V. Bagwe, M. Mondal, P. W. Adams, V. Tripathi, and P. Raychaudhuri, Phys. Rev. B **80**, 134514 (2009).

[36] A. I. Gubin, K. S. Il'in, S. A. Vitusevich, M. Siegel, and N. Klein, Phys. Rev. B **72**, 064503 (2005).

[37] C. Gorter and H. Casimir, Physica (Utrecht) **1**, 306 (1934).

[38] B. Mühlschlegel, Z. Phys. **155**, 313 (1959).

[39] S. P. Chockalingam, M. Chand, J. Jesudasan, V. Tripathi, and P. Raychaudhuri, Phys. Rev. B **77**, 214503 (2008).

[40] E. Silva, N. Pompeo, and O. V. Dobrovolskiy, Phys. Sci. Rev. **2**, 1 (2017).

[41] A. J. Berger, E. R. J. Edwards, H. T. Nembach, O. Karis, M. Weiler, and T. J. Silva, Phys. Rev. B **98**, 024402 (2018).

[42] E. B. Rosa, Bull. Bur. Stand. **4**, 301 (1908).

[43] J.-C. Rojas-Sánchez, N. Reyren, P. Laczkowski, W. Savero, J.-P. Attané, C. Deranlot, M. Jamet, J.-M. George, L. Vila, and H. Jaffrès, Phys. Rev. Lett. **112**, 106602 (2014).

[44] K. Gilmore, Y. U. Idzerda, and M. D. Stiles, Phys. Rev. Lett. **99**, 027204 (2007).

[45] L. Flacke, L. Liensberger, M. Althammer, H. Huebl, S. Geprägs, K. Schultheiss, A. Buzdakov, T. Hula, H. Schultheiss, E. R. J. Edwards, H. T. Nembach, J. M. Shaw, R. Gross, and M. Weiler, Appl. Phys. Lett. **115**, 122402 (2019).

[46] H. T. Nembach, T. J. Silva, J. M. Shaw, M. L. Schneider, M. J. Carey, S. Maat, and J. R. Childress, Phys. Rev. B **84**, 054424 (2011).

[47] T. Gilbert, IEEE Trans. Magn. **40**, 3443 (2004).

[48] D. Polder, Physica (Utrecht) **15**, 253 (1949).

[49] G. Ciovati, CERN Report No. JLAB-ACP-13-1743, https://doi.org/10.5170/CERN-2014-005.57, 2014.

[50] Y. Imai, H. Takahashi, K. Kitagawa, K. Matsubayashi, N. Nakai, Y. Nagai, Y. Uwatoko, M. Machida, and A. Maeda, J. Phys. Soc. Jpn. **80**, 013704 (2011).

[51] J. M. Shaw, H. T. Nembach, and T. J. Silva, Appl. Phys. Lett. **105**, 062406 (2014).

[52] C. González-Ruano, L. G. Johnsen, D. Caso, C. Tiusan, M. Hehn, N. Banerjee, J. Linder, and F. G. Aliev, Phys. Rev. B **102**, 020405(R) (2020).

[53] L. G. Johnsen, N. Banerjee, and J. Linder, Phys. Rev. B **99**, 134516 (2019).

[54] J. M. Beaujour, D. Ravelosona, I. Tudosa, E. E. Fullerton, and A. D. Kent, Phys. Rev. B **80**, 180415 (2009).

[55] S. Hirayama, S. Kasai, and S. Mitani, Jpn. J. Appl. Phys. **57**, 013001 (2018).

[56] S. Onoda, N. Sugimoto, and N. Nagaosa, Phys. Rev. Lett. **97**, 126602 (2006).

[57] L. Frangou, G. Forestier, S. Auffret, S. Gambarelli, and V. Baltz, Phys. Rev. B **95**, 054416 (2017).

[58] S. Takahashi, T. Yamashita, H. Imamura, and S. Maekawa, J. Magn. Magn. Mater. **240**, 100 (2002).

[59] F. Freimuth, S. Blügel, and Y. Mokrousov, Phys. Rev. B **92**, 064415 (2015).

[60] H. Głowiński, M. Schmidt, I. Gościańska, J.-P. Ansermet, and J. Dubowik, J. Appl. Phys. **116**, 053901 (2014).

[61] Y. A. Bychkov and É. I. Rashba, JETP Lett. **39**, 78 (1984), http://www.jetpletters.ac.ru/ps/1264/article_19121.shtml.

[62] V. Edelstein, Solid State Commun. **73**, 233 (1990).

[63] W. Yan, E. Sagasta, M. Ribeiro, Y. Niimi, L. E. Hueso, and F. Casanova, Nat. Commun. **8**, 661 (2017).

[64] T. Kimura, Y. Otani, T. Sato, S. Takahashi, and S. Maekawa, Phys. Rev. Lett. **98**, 156601 (2007).

[65] S. Takahashi and S. Maekawa, Jpn. J. Appl. Phys. **51**, 010110 (2012).

[66] S. Takahashi and S. Maekawa, J. Phys. Soc. Jpn. **77**, 031009 (2008).

[67] H. Kontani, J. Goryo, and D. S. Hirashima, Phys. Rev. Lett. **102**, 086602 (2009).

[68] S. Takahashi and S. Maekawa, Phys. Rev. Lett. **88**, 116601 (2002).

[69] K. Rogdakis, A. Sud, M. Amado, C. M. Lee, L. McKenzie-Sell, K. R. Jeon, M. Cubukcu, M. G. Blamire, J. W. A. Robinson, L. F. Cohen, and H. Kurebayashi, Phys. Rev. Mater. **3**, 014406 (2019).

[70] T. Wakamura, H. Akaike, Y. Omori, Y. Niimi, S. Takahashi, A. Fujimaki, and Y. Otani, Nat. Mater. **14**, 675 (2015).

[71] W. Bailey, P. Kabos, F. Mancoff, and S. Russek, IEEE Trans. Magn. **37**, 1749 (2001).

[72] C. Luo, Z. Feng, Y. Fu, W. Zhang, P. K. J. Wong, Z. X. Kou, Y. Zhai, H. F. Ding, M. Farle, J. Du, and H. R. Zhai, Phys. Rev. B **89**, 184412 (2014).

[73] J. Rantschler, B. Mar, J. Mallett, P. Chen, R. McMichael, and W. Egelhoff, IEEE Trans. Magn. **41**, 3523 (2005).

[74] A. Ghosh, J. F. Sierra, S. Auffret, U. Ebels, and W. E. Bailey, Appl. Phys. Lett. **98**, 052508 (2011).

[75] T. S. Suraj, M. Müller, S. Gelder, S. Geprägs, M. Opel, M. Weiler, K. Sethupathi, H. Huebl, R. Gross, M. S. Ramachandra Rao, and M. Althammer, J. Appl. Phys **128**, 083903 (2020).

[76] S. Mironov and A. Buzdin, Phys. Rev. Lett. **118**, 077001 (2017).

[77] S. Mironov, A. S. Mel'nikov, and A. Buzdin, Appl. Phys. Lett. **113**, 022601 (2018).

[78] O. V. Dobrovolskiy, R. Sachser, M. Huth, V. A. Shklovskij, R. V. Vovk, V. M. Bevz, and M. I. Tsindlekht, Appl. Phys. Lett. **112**, 152601 (2018).
[79] A. A. Awad, F. G. Aliev, G. W. Ataklti, A. Silhanek, V. V. Moshchalkov, Y. M. Galperin, and V. Vinokur, Phys. Rev. B **84**, 224511 (2011).
[80] J. A. Ouassou, W. Belzig, and J. Linder, Phys. Rev. Lett. **124**, 047001 (2020).
[81] J. J. He, K. Hiroki, K. Hamamoto, and N. Nagaosa, Commun. Phys. **2**, 128 (2019).
[82] K. M. D. Hals, Phys. Rev. B **93**, 115431 (2016).
[83] A. Vargunin and M. Silaev, Sci. Rep. **9**, 5914 (2019).